Modeling of Gibbs energies of pure elements down to 0K using segmented regression

Irina Roslyakova *[1], Bo Sundman [2], Holger Dette[3], Lijun Zhang[4], and Ingo Steinbach[1]

[1]*ICAMS, Ruhr-University Bochum, Germany*

[2]*CEA, Sacley, France*

[3]*Faculty of the Mathematics, Ruhr-University Bochum, Germany*

[4]*State Key Laboratory of Powder Metallurgy, Central South University, Changsha, P.R. China*

June 28, 2016

A novel thermodynamic modeling strategy of stable solid alloy phases is proposed based on segmented regression approach. The model considers several physical effects (e.g. electronic, vibrational etc.) and is valid from 0K up to the melting temperature. The preceding approach has been applied for several pure elements. Results show good agreement with experimental data at low and high temperatures. Since it is not a first attempt to propose a "universal" physical-based model down to 0K for the pure elements as an alternative to current SGTE description, we also compare the results to existing models. Analysis of the obtained results shows that the newly proposed model delivers more accurate description down to 0K for all studied pure elements according to several statistical tests.

*Electronic address: irina.roslyakova@rub.de; Corresponding author

1 Introduction

It is important to have an accurate description of the pure elements before starting a calculation of the thermodynamic properties and phase diagrams of alloy systems. Therefore, models for the Gibbs energy of pure elements, based on the heat capacities are one of the key components for successful thermodynamic optimization based on the CALPHAD method.

Currently in CALPHAD applications the temperature dependence of the heat capacity is described by high-order polynomials with adjustable parameters fitted to experimental data [8]. This approach to fit coefficients has been developed to cover high temperatures above 298.15K and should not be used to describe any low temperature data. The effort to extend that description to low temperatures demands more physical modeling which takes into account the available experiments and theoretical data. The CALPHAD community discussed this problem in 1995 during a Ringberg Workshop [5] and proposed a "universal" model to describe the thermodynamic properties over the whole temperature range down to 0K. This model considers several physical effects of the heat capacity. Such models should improve the present thermodynamic models used in the SGTE description of pure elements and the predictive capability of the CALPHAD method.

An attempt in this direction was performed by Chen and Sundman [6] applied to bcc, fcc, liquid and amorphous phases for the pure Fe. The more recent work in development of physical sounded models for the crystalline phase of pure elements was performed during a Ringberg Workshop'2013 by Palumbo et al. [20]. Following the ideas from [5], [6] and [20] a new model for the heat capacity of pure elements which considers several physical effects has been proposed in this work.

Moreover, we applied already existing physically-based models [5], [6] to model of the heat capacity data of the considered pure elements, Cr, Fe and Al. Afterwards all models have been compared with each other and the most appropriate model has been chosen based on the analysis of statistical goodness-of-fit measures. The model parameters associated with some physical constants have been validated with collected experimental data.

1.1 The heat capacity of pure elements

The heat capacity is a fundamental state property and describes the amount of energy needed to increase the temperature of a known quantity of material by 1 K. The heat capacity is measured in J/(mole K). Various physical contributions of the heat capacity are presented in Fig. 1. Overview of these physical effects is given in classical textbook of G. Grimvall [12].

From a mathematical point of view we are interested in the analytical form of the functions which can be used to describe temperature dependence of each physical effect drawn in Fig. 1 and the range where this effect could appear. Therefore, according to the review given in [12] three different types of the mathematical functions can be applied for the

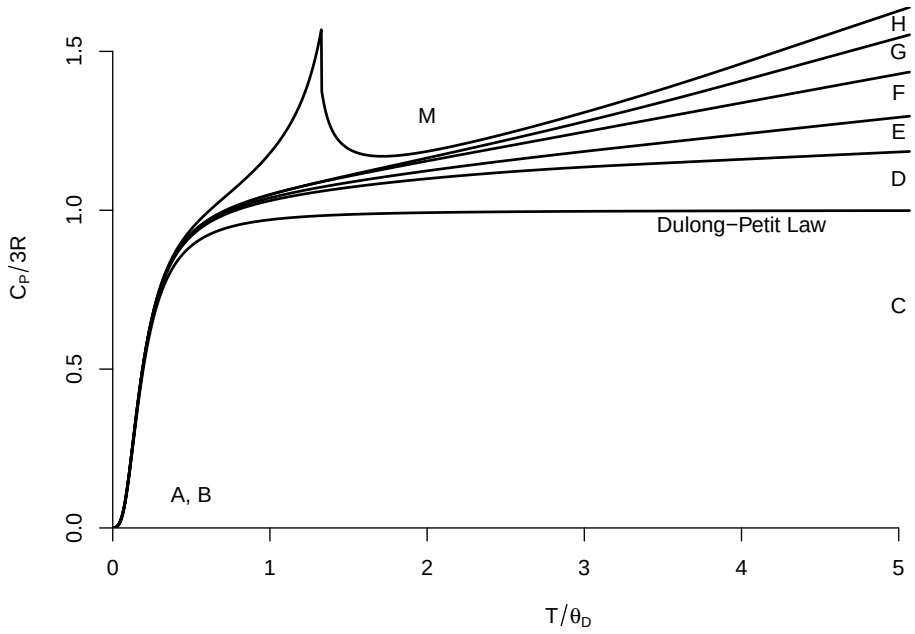

Figure 1: Physical contributions of the heat capacity: A - electronic heat capacity, B - phonon contribution, C - harmonic vibrational phonon contribution, D - $C_P - C_V$ contribution, E - explicit anharmonic contribution to C_V, F - electronic contribution, G - correction factor, H - vacancies formation, M - magnetic heat capacity

modeling of the various contributions to the heat capacity.

The main part of the heat capacity can be explained by phonon contributions (B) and the harmonic vibrational phonon contribution (C). Such effects can be described by Debye (1) or Einstein model (2) and with increase of the temperature asymptotically will reach value of $3R$ according to the Dulong-Petit law (see Fig. 2)

$$C_P^{Deb}(T,\theta_D) = 9R\Big(\frac{T}{\theta_D}\Big)^3 \int_0^{\theta_D/T} \frac{x^4 e^x}{(e^x-1)^2} dx \tag{1}$$

$$C_P^{Ein}(T,\theta_E) = 3R\Big(\frac{\theta_E}{T}\Big)^2 \frac{e^{\theta_E/T}}{(e^{\theta_E/T}-1)^2} \tag{2}$$

where θ_D and θ_E are Debye and Einstein temperature respectively.

The Debye model (1) reproduces the correct temperature dependence proportional to T^3 at very low temperatures, but has more complicated mathematical form and should be approximated by some series expansion [14], [9]. In contrast to Debye model (1), the Einstein model (2) can be easily implemented in thermodynamic databases, but it does not deliver such accurate description at the low temperatures (see Fig. 2).

The contributions to the heat capacity, (A), (D), (E), (F), and (G), presented in Fig. 1 can be modeled using linear function depending on the temperature. Two of these contributions (A) and (F) describe the effect of the electronic heat capacity at low and high temperatures correspondingly. Therefore, the linear function used for the description of the electronic C_p at low temperatures cannot be applied for the modeling of the high temperature range.

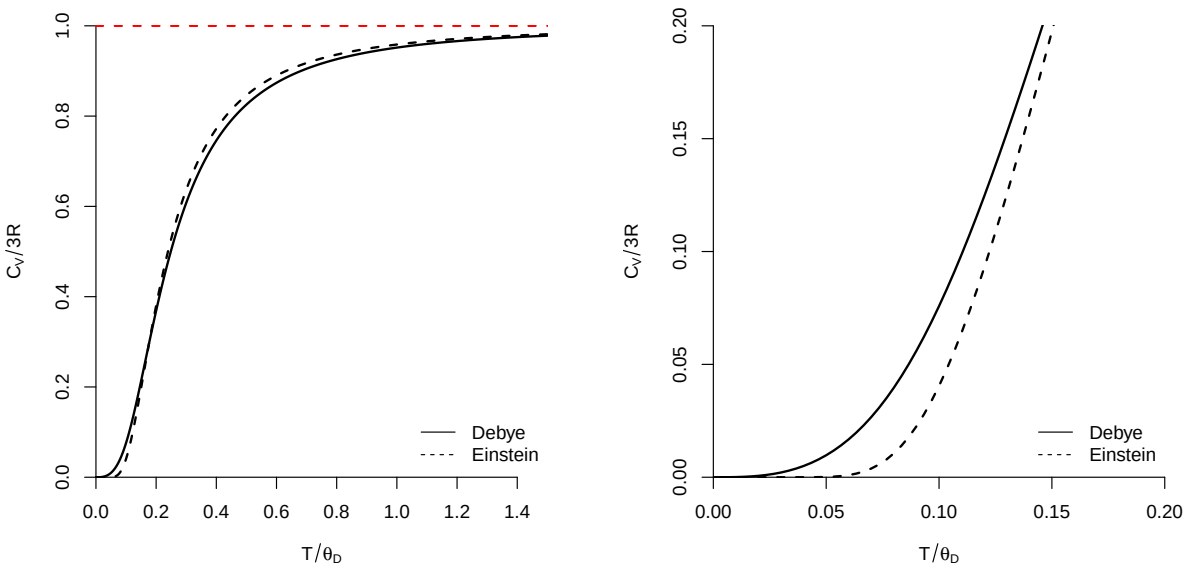

(a) low and high temperatures

(b) low temperatures

Figure 2: Debye vs. Einstein. Predicted heat capacity as a function of temperature.

The magnetic contribution (M) to the heat capacity should be considered for elements with magnetic ordering as for example Iron or Nickel. This physical effect is currently described by Inden-Hillert-Jahr model [15]. A more accurate approximation for the magnetic heat capacity has been proposed by Chen and Sundman [6] and its further improvement by Xiong et al.[26].

$$C_P^{magn} = RT \cdot g(\tau) \ln(\beta + 1), \tag{3}$$

$$g(\tau) = \begin{cases} \frac{0.63570895}{A}\left(\frac{1}{p} - 1\right)\left(2\tau^3 + 2\frac{\tau^9}{3} + 2\frac{\tau^{15}}{5} + 2\frac{\tau^{21}}{7}\right), & \tau \leq 1 \\ \frac{1}{A}\left(2\tau^{-7} + 2\frac{\tau^{-21}}{3} + 2\frac{\tau^{-35}}{5} + 2\frac{\tau^{-49}}{7}\right), & \tau \geq 1 \end{cases} \tag{4}$$

where

$$A = 0.33471979 + 0.49649686\left(\frac{1}{p} - 1\right) \tag{5}$$

Here $\tau = T/T^*$, where T^* is Curie temperature T_C for ferromagnetic materials or Neel temperature T_N for antiferromagnetic materials, β is the average magnetic momentum per atom and p is the structure factor, defined as the ratio of the magnetic enthalpy in the paramagnetic state to the total magnetic enthalpy. For the body-central cubic (bcc) structure, the accepted SGTE value is $p = 0.4$, while for the face-centered cubic (fcc) and hexagonal closed-packed (hcp) structure $p = 0.28$ is used. Chen and Sundman re-optimized the structure parameter p for the bcc phase and set its value to 0.37.

1.2 Model proposed during Ringberg Workshop'1995

The main idea behind the model proposed during a Ringberg Workshop in 1995, in the following abbreviation "RW", is based on consideration of physical contributions to the heat capacity [12] which were shortly described above. The Debye or Einstein model has

been applied to fit the heat capacity data at the low temperatures, while using a polynomial to model the temperature dependencies above 298.15K.

$$C_P^{RW}(T, \boldsymbol{\theta}^{RW}) = C_P^{Deb/Ein}(T) + aT + bT^2 + C_P^{magn}(T), \tag{6}$$

where T is temperature, $\boldsymbol{\theta}^{RW} = (\theta_D/\theta_E, a, b)$ is the vector of the unknown model parameters to be estimated, $C_P^{Deb/Ein}(T)$ is the heat capacity describing phonon contribution using Debye (1) or Einstein model (2), C_P^{magn} is magnetic contribution of the heat capacity. The parameters θ_D (or θ_E), a and b are physically motivated.

The first term $C_P^{Deb/Ein}(T)$ in the proposed model (6) is used to model the contribution from harmonic vibration. There was no concrete recommendation whether the Debye or Einstein model should be used. The second aT term in (6) is related to electronic excitations and low order aharmonic corrections. The third term bT^2 contains the next order anharmonic corrections. The last term in equation (6), $C_P^{magn}(T)$, considers the contribution from magnetic ordering.

The proposed model was applied to five pure elements Ag, Cu, Mo, Ti, Sn and one compound $CaCl_2$ and showed significant improvement of prediction quality at low temperatures [5].

1.3 Chen-Sundman model

In 2001, Chen and Sundman [6] applied a modeling concept proposed in [5] to the lattice stability of pure Fe based on Einstein model, in the following abbreviation "CS", and described C_P of the bcc phase at low temperatures by further modification of (6) into

$$C_p^{CS}(T, \boldsymbol{\theta}^{CS}) = 3R\left(\frac{\theta_E}{T}\right)^2 \frac{e^{\theta_E/T}}{(e^{\theta_E/T}-1)^2} + aT + bT^4 + C_P^{magn}(T), \tag{7}$$

where $\boldsymbol{\theta}^{CS} = (\theta_E, a, b)$ is the vector of the unknown model parameters to be estimated and $C_P^{magn}(T)$ is the magnetic contribution to the heat capacity modeled by equation (3).

They found that the 4th power of the third term would make it easier to fit the high temperature experimental data of the heat capacity for the pure Fe. They also suggested to use more terms in approximation of the Inden model (3) for description of the magnetic heat capacity [6].

The first attempt to improve the thermodynamic description of a binary system by adoption of the Chen-Sundman model (7) has been demonstrated in [27] and binary Fr-Cr phase diagram has been calculated down to 0K. The most recent application of Chen-Sundman model (7) are the calculated Fe-C binary system [19] and the thermodynamic description of pure Mn [4].

1.4 Segmented regression model for the heat capacity of pure elements

Following recommendations of Ringberg Workshop'1995 [5] and results of the work performed by Chen and Sundman [6], we propose a new model, in the following abbreviation "SR", for describing temperature dependence of the heat capacity of the pure elements, which considers relevant physical effects. Since these contributions appear in different temperature ranges [12] and can be described by different functions, the segmented regression methodology [24] was applied to develop a mathematical model for the heat capacity of the pure elements.

The proposed model for the temperature dependence of the heat capacity for pure elements consists of three terms

$$C_P^{SR}(T, \boldsymbol{\theta}^{SR}) = C_P^{Deb/Ein}(T) + C_P^{bcm}(T; \beta_1, \beta_2, \tau, \gamma) + C_P^{magn}(T), \tag{8}$$

where the first term is defined in (1) and (2), $\boldsymbol{\theta}^{SR} = (\theta_D \text{ or } \theta_E, \beta_1, \beta_2, \tau, \gamma)$ is the vector of the unknown parameters to be estimated. The second term $C_P^{bcm}(T; \beta_1, \beta_2, \tau, \gamma)$ is used for the decomposition of physical effects described by linear functions at low and high temperatures. For this purpose we used the bent-cable model,

$$C_P^{bcm}(T; \beta_1, \beta_2, \tau, \gamma) = \beta_1 T + \beta_2 \cdot q(T; \tau, \gamma), \tag{9}$$

where the term q is defined by

$$q(T; \tau, \gamma) = \frac{(T - \tau + \gamma)^2}{4\gamma} \mathbb{1}\{|T - \tau| \leq \gamma\} + (T - \tau)\mathbb{1}\{T > \tau + \gamma\}. \tag{10}$$

and $\mathbb{1}\{\cdot\}$ is indicator function, e.g. $\mathbb{1}\{T > \tau + \gamma\} = 1$ if $T > \tau + \gamma$ and 0 otherwise. Graphically, the bent-cable model is presented in Fig. 3.

The bent-cable model (9) is a continuous segmented model with four parameters $\beta_1, \beta_2, \tau, \gamma$. The incoming linear phase has a slope of β_1 and a intercept 0. The outgoing linear phase has a slope of $\beta_1 + \beta_2$ and intercept of $-\beta_2\tau$. These two linear segments are smoothly jointed in the points $\tau - \gamma$ and $\tau + \gamma$ by quadratic bend with half-weight $\gamma > 0$. If $\gamma = 0$, then the bent-cable model reduces to a non-differentiable broken stick that is plotted on the left side of Fig. 4a. For large values of γ the bent-cable model approximates into the well-known quadratic model that is presented on right side of Fig. 4b.

1.5 Statistical approach for the model selection

An important aspect of approach proposed in this paper is the consistent application of statistical methodology to optimize the free parameters of the model and to select the most appropriate model that accurately describes the experimental data with a good predictive properties. Usually, physical based models are preferred to any formal mathematical de-

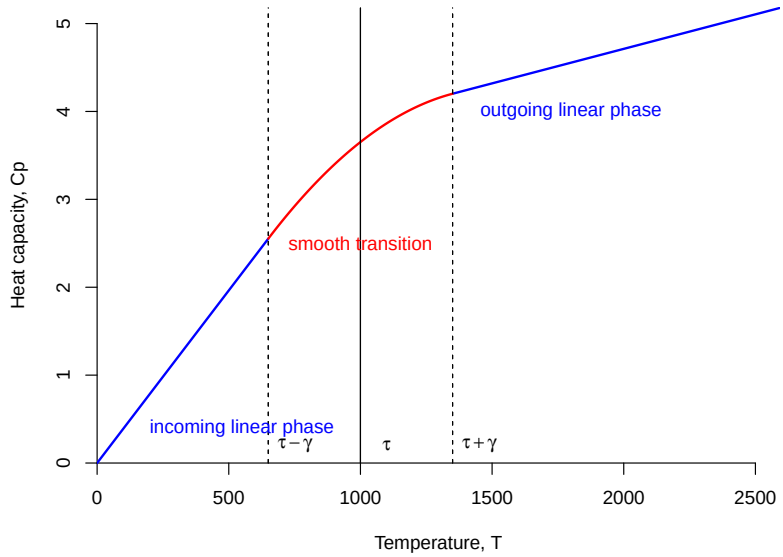

Figure 3: The full bent-cable model (9)

scription. In the ideal case, the investigator who collects or generates the data should use an appropriate model for the specific of the experiment. If it is not possible to decide which model is the most appropriate based on the expert knowledge, some kind of quantitative statistical measure can be applied to compare competing models.

Usually the parameters in a given model are estimated by the least squares method, which determines parameter values, say $\hat{\boldsymbol{\theta}}_n$, minimizing the residual sum of squares over parameter space Θ that is

$$\hat{\boldsymbol{\theta}}_n = \arg\min_{\boldsymbol{\theta}\in\Theta} \sum_{i=1}^{n} (y_i - C_P(T_i, \boldsymbol{\theta}))^2. \tag{11}$$

Here n is a number of observations and y_i and $C_P(T_i, \boldsymbol{\theta})$ are experimental and estimated values of the heat capacity at the temperature T_i, $i = 1, ..., n$.

The goodness-of-fit statistics are now calculated for each considered model (6)-(8). One of such statistics that are quite often used for a comparison of different fits is the residual standard error (RSE), which is a measure between the data and fitted regression curve defined as

$$RSE^j = \sqrt{\frac{\sum_{i=1}^{n} (y_i - C_P^j(T_i, \hat{\boldsymbol{\theta}}_n^j))^2}{n - p^j - 1}}. \tag{12}$$

Here $C_P^j(T_i, \hat{\boldsymbol{\theta}}_n^j)$ is the estimated heat capacity at temperature T_i with jth model and p^j is the number of the parameters and $\hat{\boldsymbol{\theta}}_n^j$ is the vector of the estimated parameters in the jth model. The upper index $j \in \{SR, CS, RW\}$ denotes the model under consideration when SR, CS and RW denote the segmented regression, Chen-Sundman and the Ringberg models respectively.

Alternative measures of goodness-of-fit are Akaike's information criteria (AIC) and the

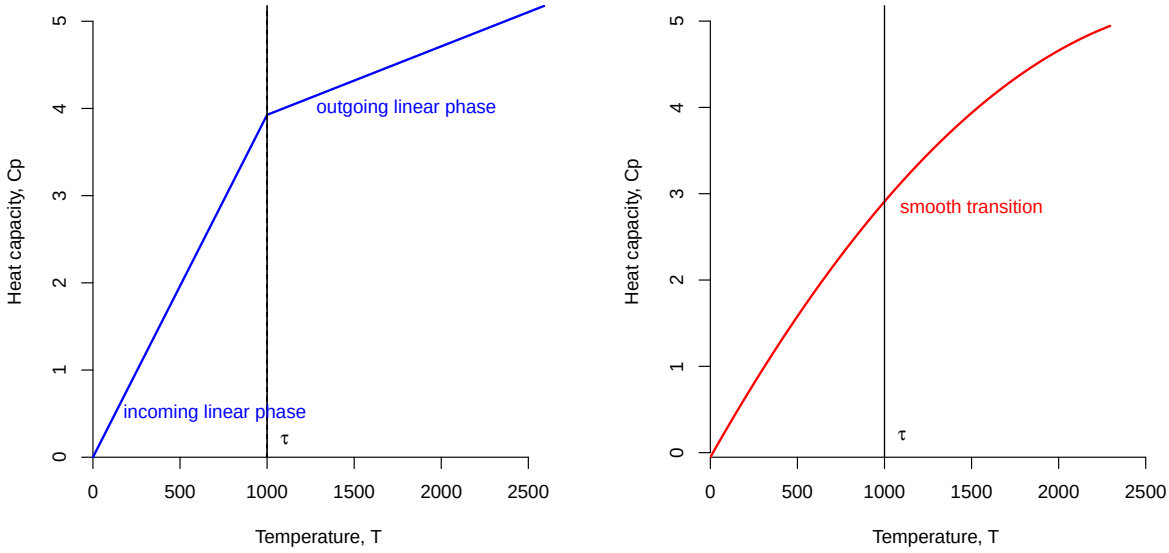

(a) $\gamma = 0$ (b) $\gamma \to \infty$

Figure 4: The bent-cable model: partial cases

Bayesian information criteria (BIC) defined as

$$AIC^j = n \ln \sum_{i=1}^{n} (y_i - C_P^j(T_i, \hat{\boldsymbol{\theta}}_n^j))^2 + p^j, \tag{13}$$

$$BIC^j = n \ln \sum_{i=1}^{n} (y_i - C_P^j(T_i, \hat{\boldsymbol{\theta}}_n^j))^2 + p^j \ln n. \tag{14}$$

Compared to the RSE-criterion the AIC and BIC criteria have the advantage that the model complexity (here the number of parameters p^j) is taken into account as penalty term. Thus one tries to find a model with a small residual standard error and a small number of parameters. This could prevent the so-called the effect of overfitting [23].

The decision rule is quite simple for all these criteria. The model with the smallest value of statistic is the most appropriate one. The measures RSE (12), AIC (13) and BIC (14) have been used in this work as objective goodness-of-fit measures for selection of the most appropriate model from statistical points of view.

2 Test of the segmented regression approach

The results for each selected pure element Cr, Al and Fe will be reported in following manner. The estimates of the model parameters with the corresponding confidence intervals are displayed in several tables. The 95%-confidence interval for rth component of the parameter vector $\boldsymbol{\theta} = (\theta_r), r = 1, ..., p$ is of the form

$$\mathrm{CI}[\theta_r] = \hat{\theta}_r \pm t_{n-p}^{0.975} \cdot \hat{s}_{\theta_r} \tag{15}$$

where $t_{n-p}^{0.975}$ is the upper 0.975 quantile of the t-distribution with $n-p$ degrees of freedom and $\hat{s}_\theta$ is the standard error of $\hat{\theta}_r$ [24].

The width of the confidence region is closely related to the sample size. Rough speaking a large confidence interval means that absolute error of estimate is large. Conversely a narrow confidence interval means that the absolute error of the parameter is small. If a confidence interval contains the values 0 this means that the corresponding parameter is not significant. In regression analysis this means that corresponding parameter could be eliminated from the considered model.

Analogously to the confidence intervals for the parameters $\theta_r, r = 1, ..., p$ of the regression model, a 95% pointwise condifence interval for the modeling function $C_P(T_i, \boldsymbol{\theta})$ can be computed as follows

$$\mathrm{CI}[C_P(T_i, \theta)] = C_P(T_i, \hat{\theta}) \pm t_{n-p}^{0.975} \cdot \hat{s}_{C_P}, \tag{16}$$

where $\hat{s}_{C_P}$ is the standard error of the estimate $C_P(T_i, \hat{\theta})$.

For a prediction of a new observation at temperature T_i one usually uses a prediction interval which is defined by

$$\mathrm{PI}[C_P(T_i, \theta)] = C_P(T_i, \hat{\theta}) \pm t_{n-p}^{0.975} \left((RSE)^2 + \hat{s}_{C_P}^2\right)^{1/2}, \tag{17}$$

where RSE is defined in (12).

Similar calculations and analysis of the reported results have been performed also with the models (6) and (7). In a second step the obtained fits have been compared visually on the basis of the RSE, AIC and BIC criteria in order to find the most appropriate model. This is defined as model for which at least two of the three criteria are minimal. To our best knowledge this is the first attempt to compare and analyze the existing physically-based models in the literature with each other.

Moreover, taking into account that some of the estimated parameters of the proposed model (8) are physically motivated, the validation of their values has been performed based on available experimental values.

2.1 General modeling remarks

Although, it is a well-known fact that Debye model deliver a more accurate description in low temperatures, we should take into account that it is still an issue to implement Debye model in its integral form or even as a series representation in the currently used TDB format. In order to perform the thermodynamic calculation and build the phase diagram down to 0K, we need an analytical expression of the Gibbs energy. For this reason we include both models in our comparison and fitted the heat capacity data for each considered model with Debye and Einstein functions respectively. This allows us to obtain the differences in the enthalpies between the fits with Debye and Einstein for low temperatures and to justify the analytical expression of the Gibbs energy function obtained

with the SR including Einstein model (see Section 3).

For pure Cr we report results for the SR model including the Debye and Einstein function to demonstrate the differences in low temperatures. Finally, for pure Al and Fe results will only reported for the Debye function.

2.2 Programming implementation and computational remarks

The models (6), (7) and (8) have been implemented in the software language R and their parameters have been estimated using nonlinear least squared method. R is a open-source software environment for statistical computing and graphics [21]. Calculations have been performed using three R-packages: *nls*2 [13], *nlstool* [3] and *investr* [11].

Numerical integration procedure already implemented in the R allows us to use the Debye model for the phonon contribution of the heat capacity directly in its integral form. This is the first attempt to include the Debye model directly in the calculation of the thermodynamic properties. Another approach to consider phonon contributions using tabulated values of the Debye functions has been proposed by Palumbo et al. [20].

2.3 Pure chromium (Cr)

The SR model is used for a fit of the heat capacity data for the pure Cr. We did not consider the magnetic term $C_p^{magn}(T)$, because a contribution from magnetic ordering in case of the pure Cr according to [2] is not significant. The most recent investigation of the magnetic properties for the pure Cr using ab-initio calculations is reported in [16].

A comparison between the experimental and predicted heat capacities from SR model is shown in Fig. 5. The fits from the SR model show a good agreement with the experimental

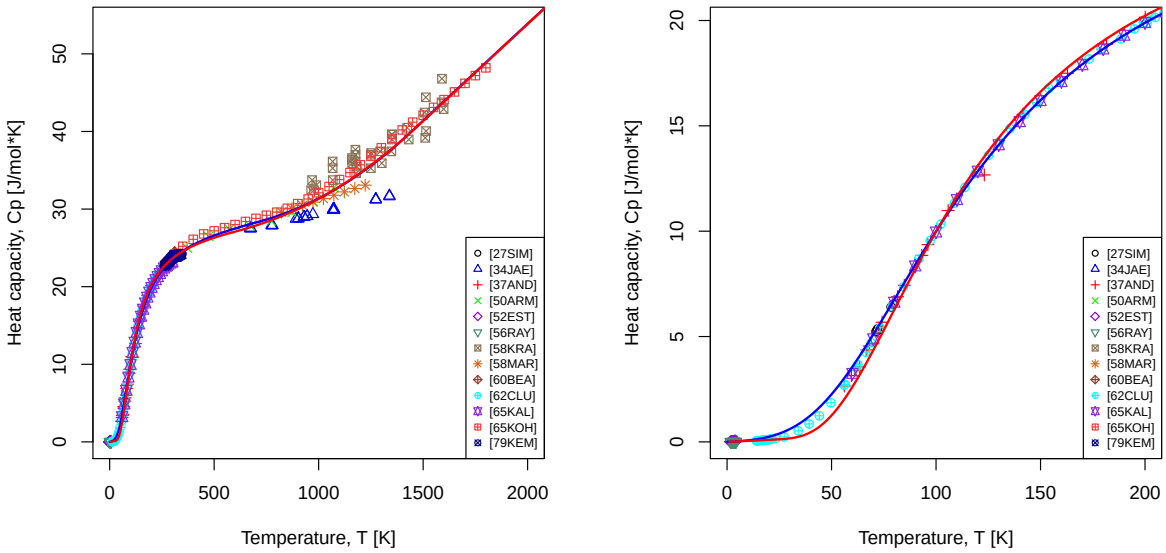

(a) low and high temperatures

(b) low temperatures

Figure 5: Fitted heat capacity of pure Cr using SR model with a Debye (blue line) and Einstein (red line) model

data over the entire temperature region (see Fig. 5a). These two fitted lines coincide almost everywhere except low temperatures (see Fig. 5b), where the combination of the bent-cable model (9) and Debye function (1) delivers more accurate description. This agrees with the classical theory on the physical effects in the heat capacity [12]. Moreover, an analysis of the measures RSE, AIC and BIC reported in Tab. 3 confirms this fact as well. The minimal values of all calculated goodness-of-fit measures are achieved for the SR model. The values of estimated models parameters with their confidence intervals for the SR model (8) are given in Tab. 2. To evaluate the uncertainties of the fitted SR model with a Debye, the confidence and prediction intervals defined in (16) and (17) are displayed on Fig. 6a and Fig. 6b respectively.

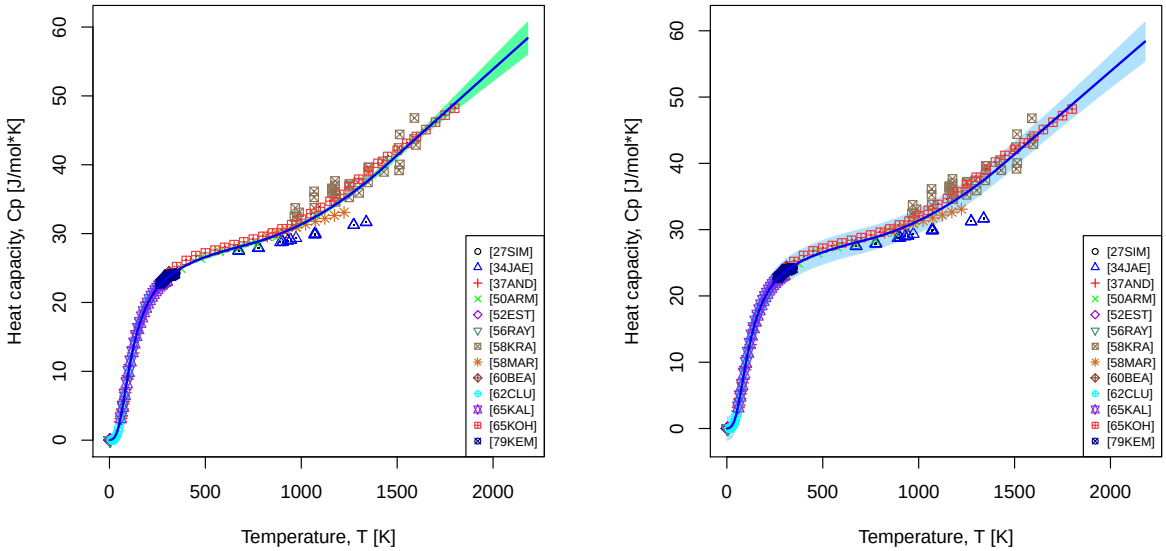

(a) Confidence band (b) Prediction band

Figure 6: Fitted by SR model (8) heat capacity of pure Cr with the confidence and prediction intervals

Author	Reference	θ_D, K	calc. θ_E,K	T, K
Andersson (1937)	[1]	485	346 (c)	56 - 300
Esterman (1952)	[10]	418±20	298 (c)	1.8 - 4.2
Wolcott (1952)	[25]	585-564	418-403 (c)	0 - 20
Rayne (1956)	[22]	630±30	450 (c)	1.5 - 4.2
Clusius (1962)	[7]	580	414 (c)	14 - 22
- Franzosini		493±6	352 (c)	> 100
Levant (1990)	[17]	510±20	364 (c)	10 - 297
This work				
- BCM with Debye		493 [480, 506]	352 (c)	entire range
- BCM with Einstein		499 (c)	356 [347, 366]	entire range

Table 1: Fitted by SR (8) and experimental values of θ_D, K of pure Cr

The obtained values for such physical parameters as the Debye θ_D temperature together with several collected experimental data are reported in Tab. 1. Einstein temperature θ_E has been evaluated using the well-known relationship $\theta_D \approx 0.714\theta_E$ given in [6]. Note that

the differences in estimated parameters values between the two SR models are insignificant (see Tab. 2) which verifies the consistency of the performed calculations. Analysis of these values shows that both θ_D and θ_E are strongly dependent on the temperature range selected for the investigation. The calculated Debye tempature is in good agreement with values reported in [1], [7] and [17], who used larger temperature ranges for their calculations as other authors (see [10], [25], [22] and [7]). The contributions of each component of the SR model is illustrated in Fig. 7.

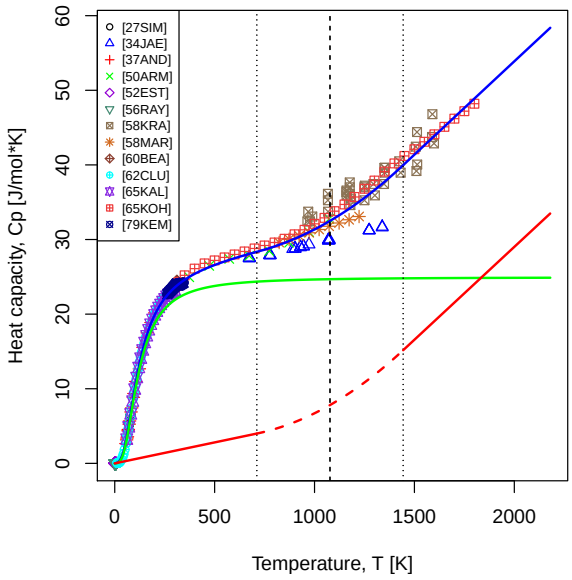

Figure 7: Components of the SR model for pure Cr. Blue line: $C_p^{Deb}(T, \hat{\theta}_D) + C_p^{bcm}(T; \hat{\beta}_1, \hat{\beta}_2, \hat{\tau}, \hat{\gamma})$, green line: $C_p^{Deb}(T, \hat{\theta}_D)$, red line: $C_p^{bcm}(T; \hat{\beta}_1, \hat{\beta}_2, \hat{\tau}, \hat{\gamma})$ (solid red lines: linear segments, dashed red line: quadratic segment)

In addition to the fitting of the experimental heat capacity data by the SR model (8), the RW (6) and CS (7) models have been applied and compared with results for pure Cr reported above. The estimated parameters values with corresponding confidence intervals for CS and RW models are presented in Tab. 2.

In Fig. 8 and Fig. 9 we compare the SR model with the two alternative physically-based models (7) and (6) could not provide the same level of the accuracy as the proposed SR model in particular in the medium and high temperature range (see Fig. 8b and Fig. 9b). On the other hand, in the low temperature all models yield similar results. The calculated heat capacity is slightly underestimated by the RW model in the middle and high temperature range (see Fig. 9) and the CS model overestimates in the high temperature region (see Fig. 8a). The visual advantages of the new SR model are confirmed by a quantitative comparison on the basis of the goodness-of-fit measures RSE, AIC and BIC introduced in Section 1.5, which are summarized in Tab. 3. We observed that the SR model (8) with Debye term is most appropriate for modeling the heat capacity of pure Cr. The second most appropriate model is the SR with Einstein function.

For completeness the SR model with Einstein function has been included in Tab. 3. We observed a larger RSE that compared to the SR model with Debye term, which is

Model	Parameter	incl. Debye term			incl. Einstein term		
		Value	Confidence Interval		Value	Confidence Interval	
			2.5%	97.5%		2.5%	97.5%
SR	$\hat{\theta}_D$ (or $\hat{\theta}_E$)	493.20	484.34	502.01	356.40	350.16	362.73
	$\hat{\beta}_1 \cdot 10^3$	5.456	4.99	5.925	4.779	4.270	5.288
	$\hat{\beta}_2 \cdot 10^2$	1.942	1.57	2.312	2.010	1.591	2.430
	$\hat{\tau}$	1072	982.09	1162.68	1035	926	1144
	$\hat{\gamma}$	372.60	225.29	519.91	441.5	282.42	600.65
CS	$\hat{\theta}_D$ (or $\hat{\theta}_E$)	492.20	484.54	499.91	359.90	354.430	365.363
	$\hat{a} \cdot 10^3$	5.325	5.045	5.604	5.140	4.861	5.419
	$\hat{b} \cdot 10^{12}$	1.569	1.463	1.676	1.642	1.535	1.749
RW	$\hat{\theta}_D$ (or $\hat{\theta}_E$)	463.70	454.56	472.94	338.30	332.31	344.38
	$\hat{a} \cdot 10^3$	1.244	0.640	1.848	0.747	0.186	1.309
	$\hat{b} \cdot 10^6$	6.183	5.704	6.662	6.587	6.139	7.035

Table 2: Pure Cr: The estimated parameters values with corresponding confidence intervals of SR, CS and RW models

consistent with the fact that the Einstein model cannot describe the low temperatures regime correctly. Only the RW model shows a lower RSE with Einstein instead of Debye in general, which shall not be analyzed here further. In the future we will only consider the Debye model as the "optimal" choice. Only for reason of numeric efficiency the use of Einstein model might be justified in high temperature regime if the low temperature error is considered in the integration constant of the Gibbs energy.

Statistics	SR		CS		RW		MA-Model	
	Debye	Einstein	Debye	Einstein	Debye	Einstein	Debye	Einstein
RSE	0.90	0.91	0.92	0.94	1.01	0.98	SR	SR
AIC	1170	1183	1194	1210	1274	1245	SR	SR
BIC	1194	1207	1210	1226	1290	1262	SR	SR

Table 3: Calculated RSE, AIC, BIC statistics for the SR, CS and RW models and the selected most appropriate model (MA-Model) for pure Cr

2.4 Pure aluminum (Al)

In this section we investigate the performance of the different models analyzing the heat capacity data for pure Al. As pure Al is nonmagnetic, we use $C_p^{magn}(T) = 0$ for all models.

We observe from Fig. 10 that the new SR model provides a very good fit of the experimental data for the entire temperature range (Fig. 10a) and the main part of the low temperature region (Fig. 10b). The estimated parameter values with corresponding confidence intervals for the fitted SR are reported in Tab. 4.

The different components C_P^{Deb} and C_P^{bcm} of the SR are displayed in Fig. 11 while the corresponding confidence and prediction intervals are shown on Fig.12a and Fig.12b respectively.

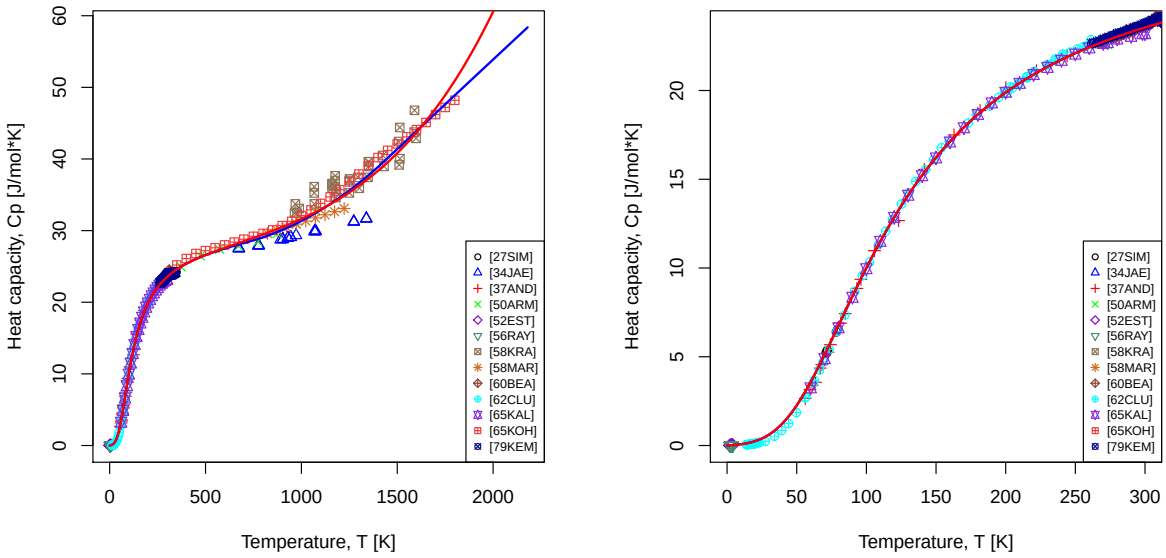

(a) entire temperature range (b) low temperatures

Figure 8: Comparison of the fitted SR and CS models for pure Cr. Blue line: the SR model, red line: the CS model.

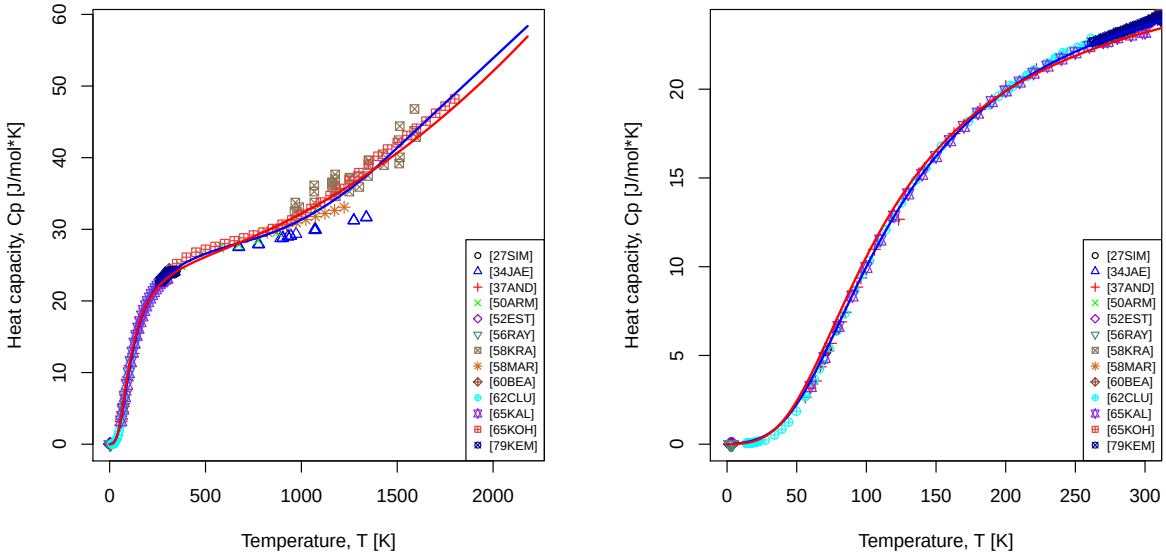

(a) entire temperature range (b) low temperatures

Figure 9: Comparison of the fitted SR and RW models for pure Cr: Blue line: the SR model, red line: the RW model

In Fig. 13 and 14 we compare the new SR model with the RW and CS models. The fitted heat capacity with the RW and SR models deliver similar results and describe experimental data well over entire temperature range (see Fig.14a). In contrast, the CS model slightly overestimates the experimental heat capacity data in the high temperatures which is demonstrated on Fig.13a. This fact also has been confirmed by analysis of the selected goodness-of-fit measures, RSE, AIC and BIC. The minimal values of all selected measures belong to the SR model. The estimated parameters with the corresponding confidence intervals for the RW and CS models are reported in Tab. 4.

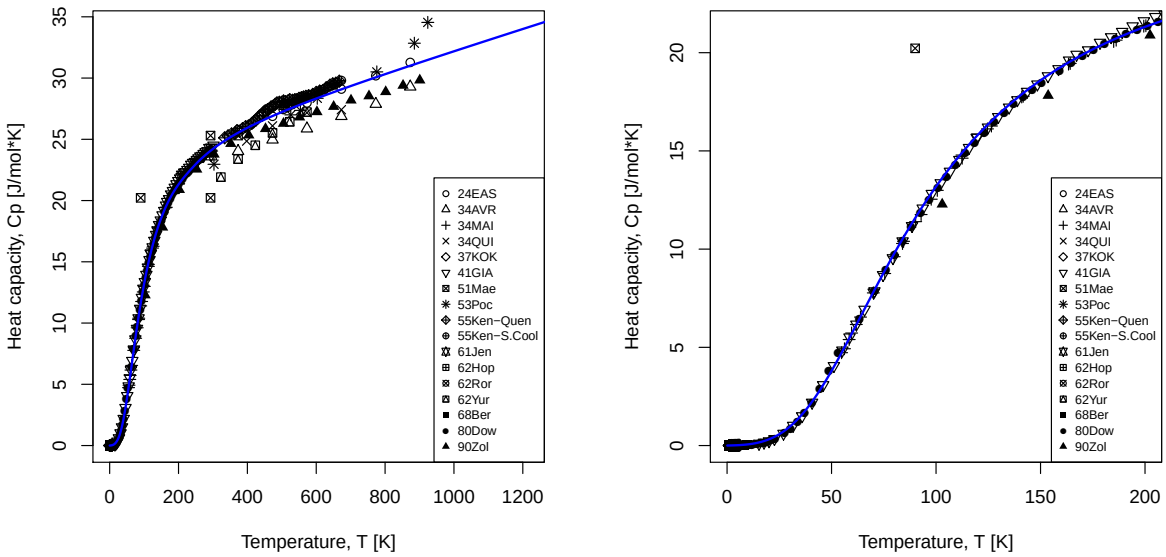

(a) low and high temperatures (b) low temperatures

Figure 10: Fitted heat capacity of pure Al using SR model

Model	Parameter	incl. Debye term			incl. Einstein term		
		Value	Confidence Interval		Value	Confidence Interval	
			2.5%	97.5%		2.5%	97.5%
SR	$\hat{\theta}_D$ (or $\hat{\theta}_E$)	390.30	382.84	397.75	280.70	272.97	288.48
	$\hat{\beta}_1 \cdot 10^3$	2.724	0.961	4.488	0.326	-3.537	4.188
	$\hat{\beta}_2 \cdot 10^3$	6.090	4.084	8.095	9.446	5.310	13.581
	$\hat{\tau}$	227.00	164.56	289.44	215.20	134.13	296.31
	$\hat{\gamma}$	21.67	-253.60	296.94	75.79	-79.21	230.80
CS	$\hat{\theta}_D$ (or $\hat{\theta}_E$)	403.80	399.24	408.33	294.50	291.08	297.90
	$\hat{a} \cdot 10^3$	5.315	4.959	5.671	5.002	4.617	5.387
	$\hat{b} \cdot 10^6$	3.304	2.243	4.364	4.133	2.974	5.292
RW	$\hat{\theta}_D$ (or $\hat{\theta}_E$)	396.50	391.48	401.54	288.00	284.34	291.63
	$\hat{a} \cdot 10^3$	3.047	2.246	3.848	2.051	1.213	2.889
	$\hat{b} \cdot 10^6$	5.191	3.914	6.468	6.712	5.364	8.059

Table 4: Pure Al: The estimated parameters values with corresponding confidence intervals of SR, CS and RW models

Statistics	SR		CS		RW		MA-Model	
	Debye	Einstein	Debye	Einstein	Debye	Einstein	Debye	Einstein
RSE	0.631	0.665	0.658	0.726	0.643	0.698	SR	SR
AIC	963	1016	1003	1102	980	1063	SR	SR
BIC	988	1041	1020	1118	997	1080	SR	SR

Table 5: The calculated goodness-of-fit measures, RSE, AIC and BIC, for the SR, CS and RW models fitted to pure Al data

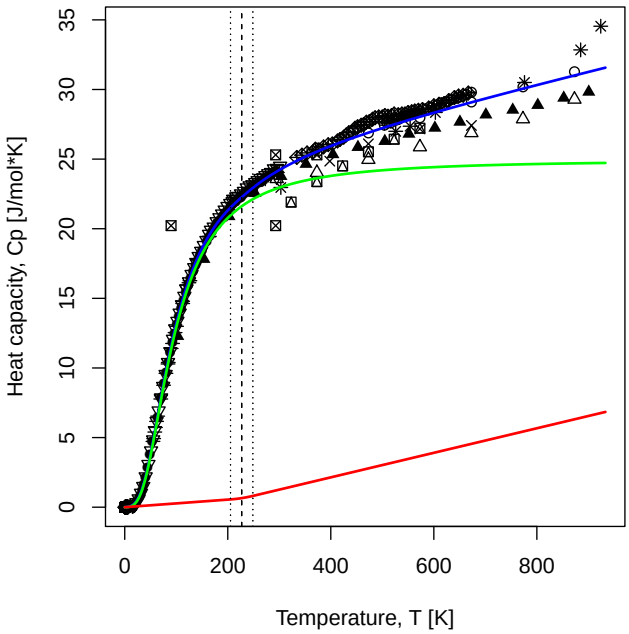

Figure 11: Components of the SR model for pure Al. Blue line: $C_p^{Deb}(T, \hat{\theta}_D) + C_p^{bcm}(T; \hat{\beta}_1, \hat{\beta}_2, \hat{\tau}, \hat{\gamma})$, green line: $C_p^{Deb}(T, \hat{\theta}_D)$, red line: $C_p^{bcm}(T; \hat{\beta}_1, \hat{\beta}_2, \hat{\tau}, \hat{\gamma})$ (solid red lines: linear segments, dashed red line: quadratic segment)

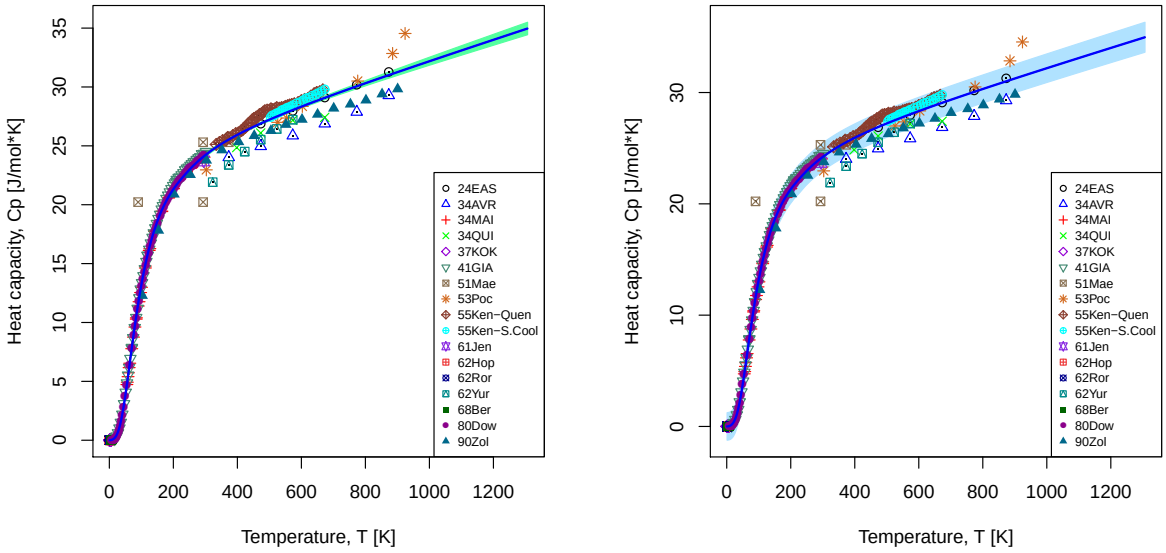

(a) Confidence band

(b) Prediction band

Figure 12: Fitted by SR model heat capacity of pure Al with the corresponding confidence and prediction intervals

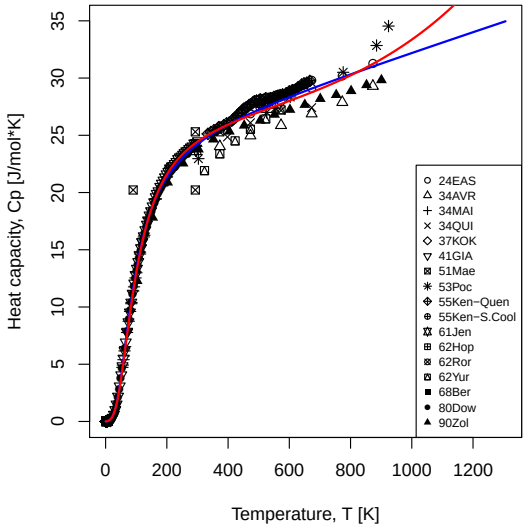

(a) entire temperature range

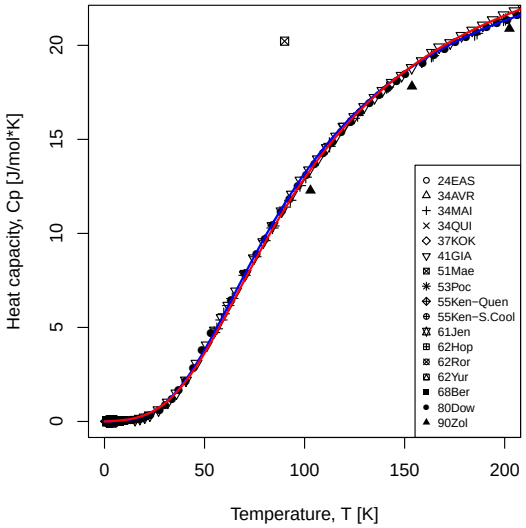

(b) low temperatures

Figure 13: Comparison of the fitted SR and CS models. Blue line: the SR model, red line: the CS model.

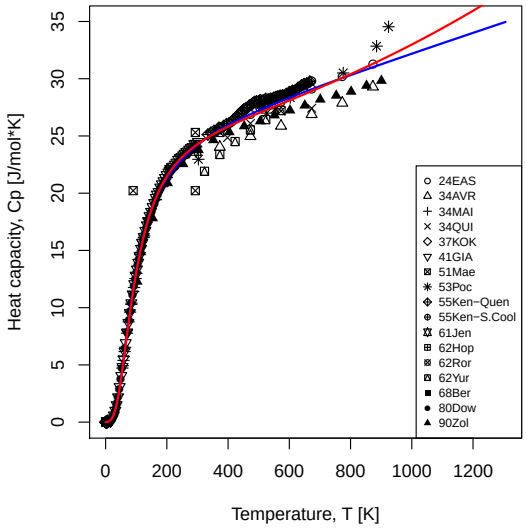

(a) entire temperature range

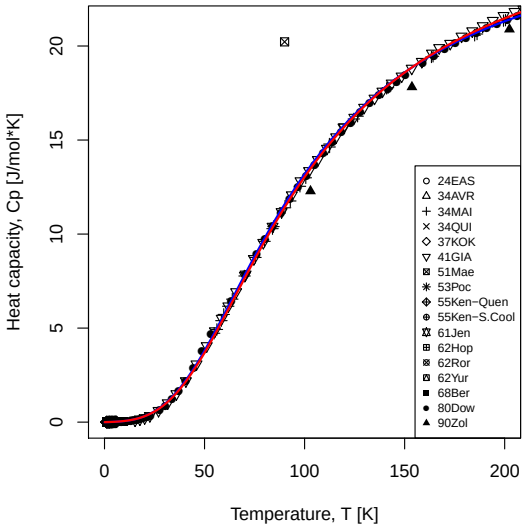

(b) low temperatures

Figure 14: Comparison of the fitted SR and RW models. Blue line: the SR model, red line: the RW model.

2.5 Pure iron (Fe)

In this section we compare the different approaches modeling the heat capacity data for pure Fe where we include a magnetic effect in all models which has been described by equation (3) in Chen and Sundman [6]. In Fig. 15 we show the results for the new SR model and observe a reasonable fit in the low and high temperature regions. The estimated

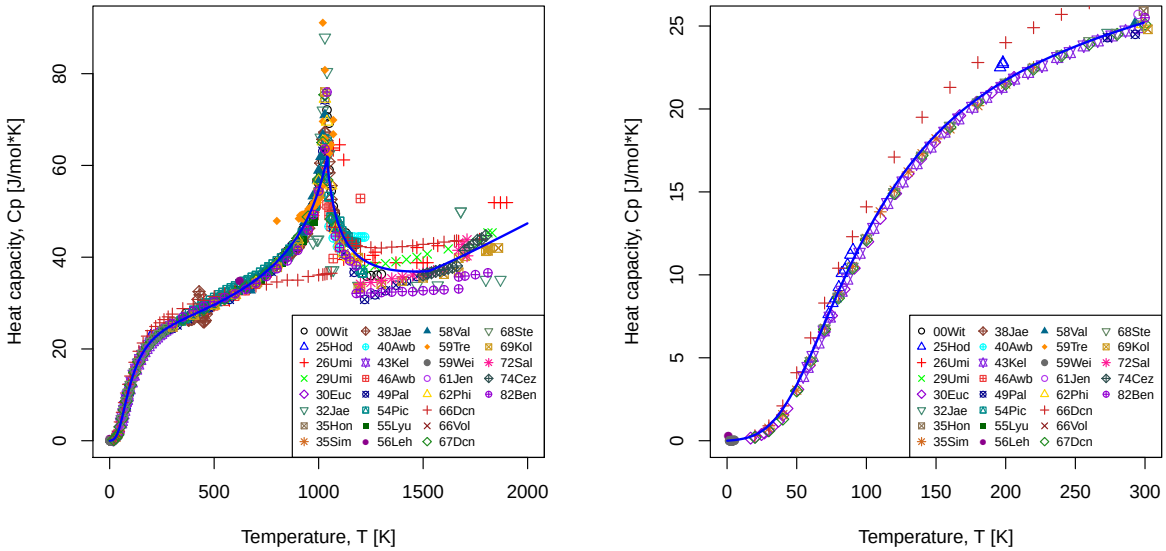

(a) low and high temperatures

(b) low temperatures

Figure 15: Fitted heat capacity of pure Fe using the SR model

parameter values together with their confidence intervals in the SR model are reported in Tab.6. The parameter values from the fit of the SR model with Debye term do not differ substantially from these SR model with Einstein function which confirms a consistency of our calculations. Values of such physical parameters as Debye θ_D temperature have been compared with each other using a well-known relationship $\theta_D \approx 0.714\theta_E$ given in [6].

Model	Parameter	incl. Debye term			incl. Einstein term		
		Value	Confidence Interval		Value	Confidence Interval	
			2.5%	97.5%		2.5%	97.5%
SR	$\hat{\theta}_D$ (or $\hat{\theta}_E$)	421.50	393.05	449.93	307.80	288.34	327.34
	$\hat{\beta}_1 \cdot 10^3$	7.177	6.770	7.584	7.218	6.811	7.624
	$\hat{\beta}_2 \cdot 10^3$	1.683	0.242	3.124	1.676	0.232	3.120
	$\hat{\tau}$	1526	1333.40	1719.11	1525	1330.46	1720.14
	$\hat{\gamma}$	85.72	-530.68	702.13	87.23	-528.51	702.96
CS	$\hat{\theta}_D$ (or $\hat{\theta}_E$)	417.60	389.08	446.11	305.40	285.83	324.92
	$\hat{a} \cdot 10^3$	6.668	6.121	7.215	6.704	6.159	7.249
	$\hat{b} \cdot 10^6$	4.237	2.459	6.013	4.263	2.489	6.037
RW	$\hat{\theta}_D$ (or $\hat{\theta}_E$)	412.50	383.50	441.59	301.80	281.98	321.64
	$\hat{a} \cdot 10^3$	5.422	4.211	6.632	5.418	4.217	6.619
	$\hat{b} \cdot 10^6$	1.822	0.892	2.751	1.860	0.935	2.784

Table 6: Pure Fe: The estimated parameters values with corresponding confidence intervals of the SR, CS and RW models

The different components of the SR model are displayed in Fig. 16 while the confidence and prediction intervals are shown on Fig. 17a and Fig. 17b respectively. The confidence

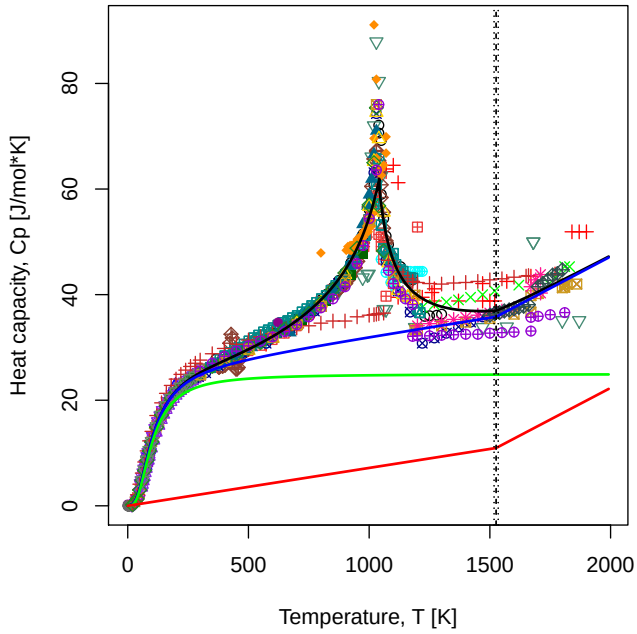

Figure 16: Components of the SR model. Black line: $C_p^{Deb}(T,\hat{\theta}_D) + C_p^{bcm}(T;\hat{\beta}_1,\hat{\beta}_2,\hat{\tau},\hat{\gamma}) + C_p^{magn}(T)$, blue line: $C_p^{Deb}(T,\hat{\theta}_D) + C_p^{bcm}(T;\hat{\beta}_1,\hat{\beta}_2,\hat{\tau},\hat{\gamma})$, green line: $C_p^{Deb}(T,\hat{\theta}_D)$, red line: $C_p^{bcm}(T;\hat{\beta}_1,\hat{\beta}_2,\hat{\tau},\hat{\gamma})$ (solid red lines: linear segments, dashed red line: quadratic segment)

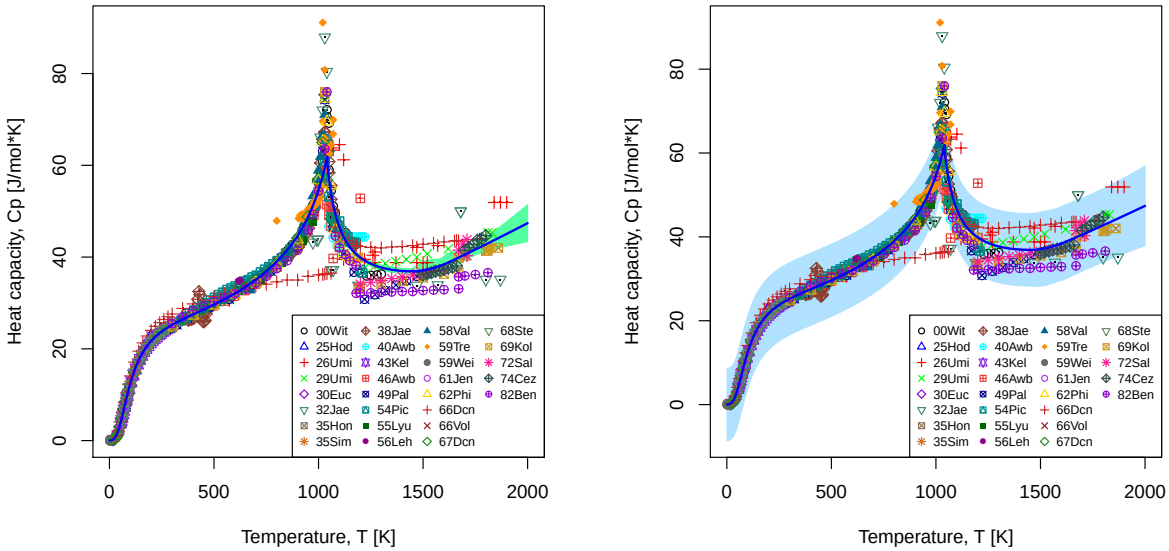

(a) Confidence band

(b) Prediction band

Figure 17: Fitted heat capacity by SR model with the corresponding confidence and prediction intervals

interval presented in Fig.17a is narrow and the fitted SR has been estimated precisely. The prediction intervals covers almost all experimental heat capacity data of pure Fe and shows a range where a new data point could appear. Since the experimental data used for the fitting are strongly heterogeneous and in some cases even contradictory to each other, it is not surprising that we obtain larger prediction interval for pure Fe as in case of Cr and Al.

Next we compare the CS and RW models with the new SR model. The estimated parameters with the confidence intervals for these models are reported in Tab. 6 and the corresponding fits are shown in Fig. 19 and Fig.18. The CS model and the SR deliver similar results and describe experimental data well in low and high temperature ranges (see Fig.18). In contrast, the RW model slightly underestimates heat capacity data in middle temperature range (see Fig.18a).

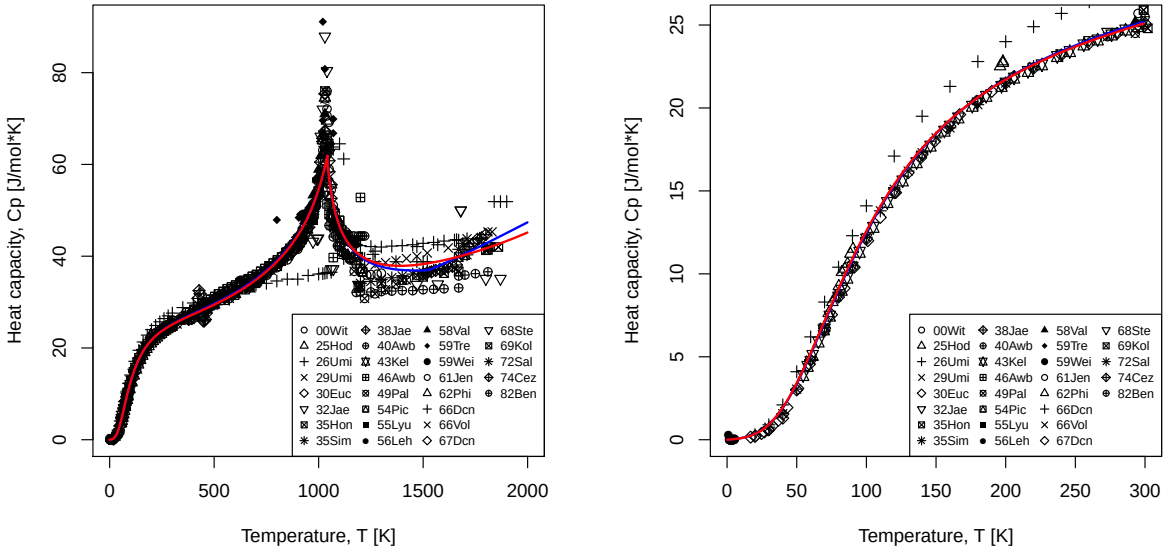

(a) entire temperature range (b) low temperatures

Figure 18: Comparison of the fitted SR and CS models for pure Fe: Blue line: the SR model, red line: the CS model.

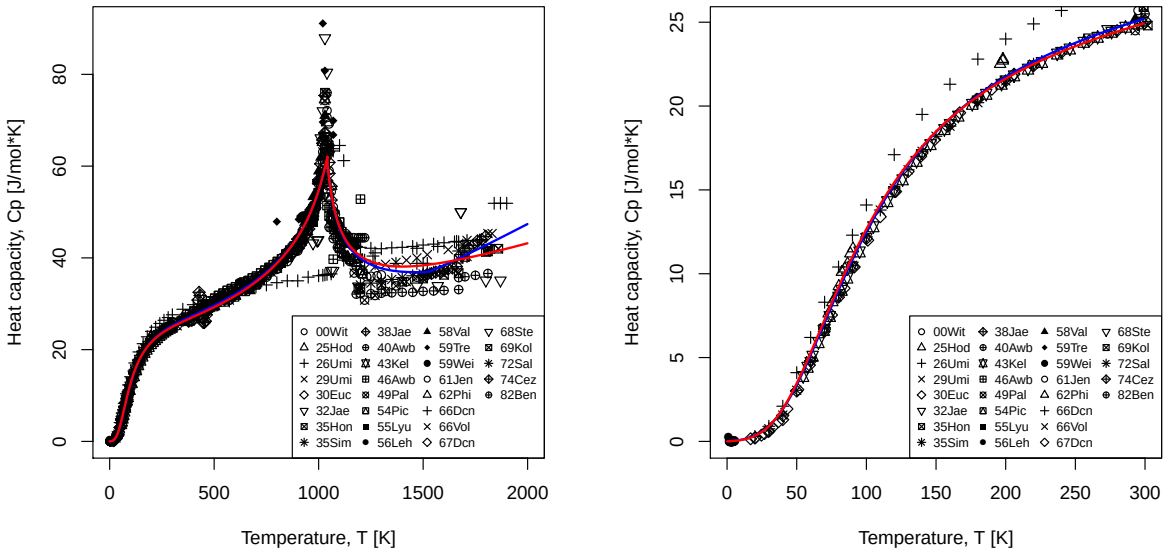

(a) entire temperature range (b) low temperatures

Figure 19: Comparison of the fitted SR and RW model for pure Fe. Blue line: the SR model, red line: the RW model.

The analysis of the RSE, AIC and BIC for the different models confirms this conclusion from visual inspection. The SR model has been selected as the most appropriate model for the fitting of the heat capacity data of pure Fe according to the minimal values of the RSE

and AIC measures. However, according to the analysis of the obtained BIC values, the CS model also has been identified as a reasonable function. However, this is not a surprising observation as initially the CS model has been developed for modeling the heat capacity of pure Fe. It is therefore remarkable that the SR model provides the same accuracy as the CS model.

Statistics	SR		CS		RW		MA-Model	
	Debye	Einstein	Debye	Einstein	Debye	Einstein	Debye	Einstein
RSE	4.378	4.38	4.396	4.397	4.415	4.415	SR	SR
AIC	4564.4	4565.2	4568.9	4569.3	4575.9	4575.9	SR	SR
BIC	4592.5	4593.2	4587.7	4588.0	4594.6	4594.6	CS	CS

Table 7: The goodness-of-fit measures of the SR, CS and RW models for pure Fe

3 Modeling Gibbs energy by segmented regression

According to the analysis of the obtained fitted results for pure Cr, Al and Fe, the proposed SR model has been selected as the most appropriate model in comparison to other two physically-based models, CS and RW. For the considered physically-based models a more accurate description of the experimental heat capacity is provided by the Debye function. The difference between the formulations with Debye (1) and Einstein (2) is significant for low temperatures. For middle and high temperatures the Debye and Einstein functions yield similar results. Therefore, since it is still an issue to implement the Debye model into TDB format, the explicit expression for thermodynamic quantities, enthalpy $H(T)$, entropy $S(T)$ and Gibbs energy $G(T)$ will be derived for the SR model where the Einstein function is used for the description of the phonon contribution in the heat capacity.

3.1 Analytical expression of Gibbs energy, $G(T)$, for segmented regression model

The thermodynamic functions $G(T)$, $S(T)$, $H(T)$ and $C_p(T)$ provide the starting point for the construction and theoretical investigation of unary and binary phase diagrams. These properties are related by the well-known equation

$$G(T) = H(T) - T \cdot S(T), \tag{18}$$

where the enthalpy $H(T)$ and the entropy $S(T)$ can be derived from the heat capacity through the formulas

$$H(T) = \int C_p(T)dT \quad \text{and} \quad S(T) = \int \frac{C_p(T)}{T}dT \tag{19}$$

The proposed segmented model for the heat capacity (8) contains three terms

$$C_p^{SR}(T) = C_p^{Ein} + C_p^{bcm} + C_p^{magn} \tag{20}$$

where C_p^{magn} is described by (3)-(5) as proposed by Chen and Sundman [6] and

$$C_p^{Ein} = 3R\Big(\frac{\theta_E}{T}\Big)^2 \frac{e^{\theta_E/T}}{(e^{\theta_E/T}-1)^2}, \tag{21}$$

$$C_p^{bcm} = \begin{cases} \beta_1 T, & T < \alpha - \gamma \\ \beta_1 T + \beta_2 \frac{(T-\alpha+\gamma)^2}{4\gamma}, & \alpha-\gamma \le T \le \alpha+\gamma. \\ \beta_1 T + \beta_2 (T-\alpha), & \alpha+\gamma < T \end{cases} \tag{22}$$

Since Chen and Sundman provided the analytical expression for magnetic G^{magn} and Einstein G^{Ein} terms of the Gibbs energy, we just refer for more details to their paper [6]. The mathematical expression for the bent-cable term of the enthalpy is obtained from the segmented model for the heat capacity (22) using the relation (19)

$$H(T) = \begin{cases} \beta_1 \frac{T^2}{2}, & T < \alpha - \gamma \\ \beta_1 \frac{T^2}{2} + \beta_2 \frac{(T-\alpha+\gamma)^3}{12\gamma}, & \alpha-\gamma \le T \le \alpha+\gamma, \\ \beta_1 \frac{T^2}{2} + \beta_2 \frac{T(T-\alpha)}{2} + \beta_2 \Big(\frac{\gamma^2}{6} + \frac{\alpha^2}{2}\Big), & \alpha+\gamma < T \end{cases} \tag{23}$$

After the collection of the coefficients according to the same order of power for the T terms, the bent-cable part of $H(T)$ will have the following form

$$H^{bcm}(T) = \begin{cases} c_1^{(H)} T^2, & T < \alpha - \gamma \\ a_2^{(H)} + b_2^{(H)} T + c_2^{(H)} T^2 + d_2^{(H)} T^3, & \alpha-\gamma \le T \le \alpha+\gamma, \\ a_3^{(H)} + b_3^{(H)} T + c_3^{(H)} T^2, & \alpha+\gamma < T \end{cases} \tag{24}$$

where the coefficients $c_1^{(H)}, a_2^{(H)}, b_2^{(H)}, c_2^{(H)}, d_2^{(H)}, a_3^{(H)}, b_3^{(H)}, c_3^{(H)}$ are connected with the estimated parameters of the bent-cable mode $\beta_1, \beta_2, \alpha, \gamma$ by the relationship

$$\begin{aligned} &c_1^{(H)} = \frac{\beta_1}{2}, \\ &a_2^{(H)} = \frac{-\beta_2}{12\gamma}(\alpha-\gamma)^3, \quad b_2^{(H)} = \frac{\beta_2}{4\gamma}(\alpha-\gamma)^2, \quad c_2^{(H)} = \frac{\beta_1}{2} - \frac{\beta_2}{4\gamma}(\alpha-\gamma), \quad d_2^{(H)} = \frac{\beta_2}{12\gamma}, \\ &a_3^{(H)} = \frac{\beta_2}{2}\Big(\frac{\gamma^2}{3} + \alpha^2\Big), \quad b_3^{(H)} = -\beta_2\alpha, \quad c_3^{(H)} = \frac{\beta_1+\beta_2}{2}. \end{aligned}$$

Analytical expression for the entropy $S(T)$ can be derived in similar way and the second term in the expression is given for the Gibbs energy (18) by

$$T \cdot S(T) = \begin{cases} c_1^{(S)} T^2, & T < \alpha - \gamma \\ b_2^{(S)} T + c_2^{(S)} T^2 + d_2^{(S)} T^3 + e_2^{(S)} T \ln(T), & \alpha - \gamma \le T \le \alpha + \gamma, \\ b_3^{(S)} T + c_3^{(S)} T^2 + e_3^{(S)} T \ln(T), & \alpha + \gamma < T \end{cases} \tag{25}$$

where the coefficients $c_1^{(S)}, b_2^{(S)}, c_2^{(S)}, d_2^{(S)}, e_2^{(S)}, b_3^{(S)}, c_3^{(S)}, e_3^{(S)}$ are connected with the estimated parameters of the bent-cable mode $\beta_1, \beta_2, \alpha, \gamma$ by the relationship

$$\begin{aligned} c_1^{(S)} &= \beta_1, \\ b_2^{(S)} &= (\alpha-\gamma)^2\Big(\frac{3k_2}{8\gamma} - \frac{k_2}{4\gamma}\ln(\alpha-\gamma)\Big), \quad c_2^{(S)} = \beta_1 - \frac{k_2(\alpha-\gamma)}{2\gamma}, \\ d_2^{(S)} &= \frac{\beta_2}{8\gamma}, \quad e_2^{(S)} = \frac{\beta_2}{4\gamma}(\alpha-\gamma)^2 \\ b_3^{(S)} &= -\frac{3\beta_2\alpha}{2} - \frac{\beta_2}{4\gamma}\Big((\alpha-\gamma)^2\ln(\alpha-\gamma) - (\alpha+\gamma)^2\ln(\alpha+\gamma)\Big), \quad c_3^{(S)} = \beta_1 + \beta_2 \\ e_3^{(S)} &= -\beta_2\alpha. \end{aligned}$$

Therefore, the bent-cable part of the total Gibbs energy $G(T)^{bcm}$ at 101,325Pa can be evaluated from the the heat capacity $C_p(T)^{bcm}$ expression (22) using equations (18), (19) as

$$G(T) = \begin{cases} c_1 T^2, & T < \alpha - \gamma \\ a_2 + b_2 T + c_2 T^2 + d_2 T^3 + e_2 T \ln(T), & \alpha - \gamma \le T \le \alpha + \gamma. \\ a_3 + b_3 T + c_3 T^2 + e_3 T \ln(T), & T > \alpha + \gamma \end{cases} \tag{26}$$

Here coefficients $c_1, a_2, b_2, c_2, d_2, e_2, a_3, b_3, c_3, e_3$ in expression for the G^{bcm} (26) can be derived directly from the estimated values of parameters $\beta_1, \beta_2, \alpha, \gamma$

$$\begin{aligned} c_1 &= -\frac{\beta_1}{2}, \\ a_2 &= -\frac{\beta_2}{12\gamma}(\alpha-\gamma)^3, \quad b_2 = (\alpha-\gamma)^2\Big(-\frac{\beta_2}{8\gamma} + \frac{\beta_2}{4\gamma}\ln(\alpha-\gamma)\Big), \quad c_2 = -\frac{\beta_1}{2} + \frac{\beta_2}{4\gamma}(\alpha-\gamma), \\ d_2 &= -\frac{\beta_2}{24\gamma}, \quad e_2 = -\frac{\beta_2}{4\gamma}(\alpha-\gamma)^2 \\ a_3 &= \frac{1}{6}\beta_2\gamma^2 + \frac{1}{2}\beta_2\alpha^2, \quad b_3 = \frac{\beta_2\alpha}{2} + \frac{\beta_2}{4\gamma}\Big((\alpha-\gamma)^2\ln(\alpha-\gamma) - (\alpha+\gamma)^2\ln(\alpha+\gamma)\Big), \\ c_3 &= -\frac{1}{2}(\beta_1+\beta_2), \quad e_3 = \beta_2\alpha. \end{aligned}$$

3.2 Verification of results from physical point of view

The consistency of underlying fitting results from a physical point of view has been performed by calculating the relative enthalpy $H - H_{298.15}$ that can be derived directly from the fitted heat capacity $C_p(T)$ [18].

$$H(T) - H_{298.15} = \int_{298.15}^{T} C_P(T)dT \tag{27}$$

Since the proposed SR model with the Debye term (1) has been selected as the most-appropriate model for the description of the heat capacity data, we calculate relative enthalpies using equation (27) and compare it with the collected experimental data. The predicted relative enthalpies and experimental results for pure Cr, Al and Fe are presented in Fig. 20, Fig. 21 and Fig. 22 respectively. In all cases we observe good predictions by the SR model. No data on the relative enthalpy at the temperatures below 298.15K were found in the literature.

Additionally, the enthalpy $H_{298.15}$ and entropy $S_{298.15}$ at the room temperature has been calculated and compared with the values reported in [8] and [20]. The corresponding results are presented in Tab.8 which also gives a comparison with the values from SGTE description [8] for pure Al, Cr and Fe. We can observed slightly higher values of $H_{298.15}$ for all considered models (6), (7), (8). The values of standard enthalpy calculated with segmented regression model (8) are in good agreement with current SGTE data.

Reference	model	Cr bcc	Fe bcc	Al fcc
Dinsdale (1991) [8]	SGTE	4050.0	4489.0	4540.0
Present work	SR with Debye	4064.34	4583.94	4557.89
	SR with Einstein	4068.93	4598.39	4565.24
	CS with Debye	4064.46	4584.97	4579.18
	CS with Einstien	4059.18	4596.36	4583.12
	RW with Debye	4096.48	4576.04	4567.47
	RW with Einstein	4089.82	4585.27	4564.81

Table 8: Calculated standard enthalpy $H_{298.15}$

The calculated standard entropies $S_{298.15}$ for Cr bcc, Fe bcc and Al fcc in comparison with first-principles and assessed standard entropy $S_{298.15}$ from [20] are presented in Tab.9. Assessed values are from current SGTE description [8]. QE are values computed using Quantum Espresso and density functional perturbation theory, VASP are values computed using VASP and the supercell method. QHA refers to the quasiharmonic approximation, QHA+ el to the quasiharmonic approximation including the electronic contribution. For more details and description of these methods we refer to [20]. Calculations performed by integration of the SR model (8) for $C_p(T)$ from 0K up to 298 K (NLS) provide reliable results for the thermodynamic properties such as the entropy and show good agreement with first-principle calculation reported by Palumbo et al. [20]. Slightly higher values

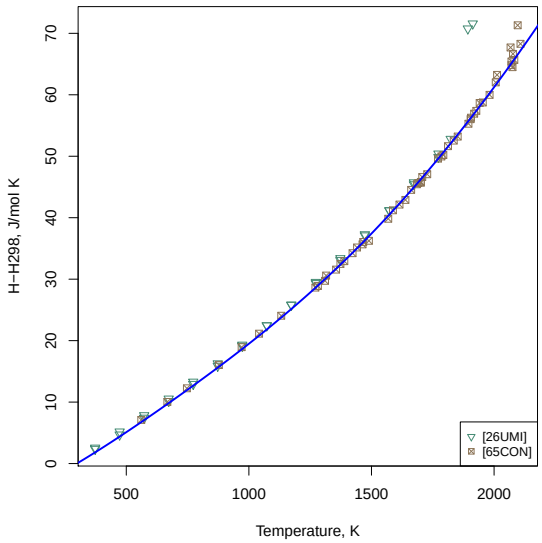

Figure 20: Calculated and experimental relative enthalpy $H - H_{298.15}$ for pure Cr

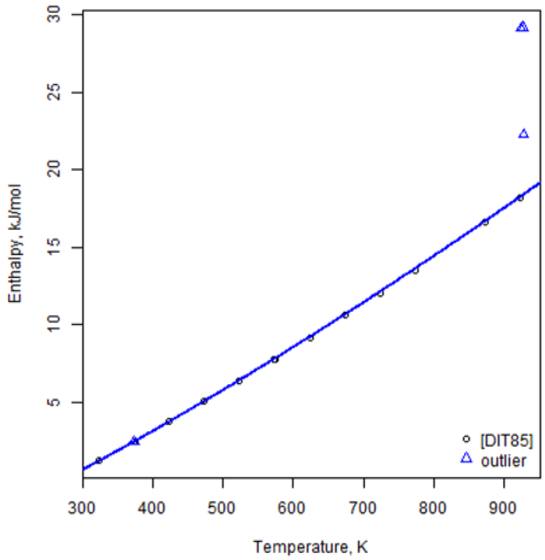

Figure 21: Calculated and experimental relative enthalpy $H - H_{298.15}$ for pure Al

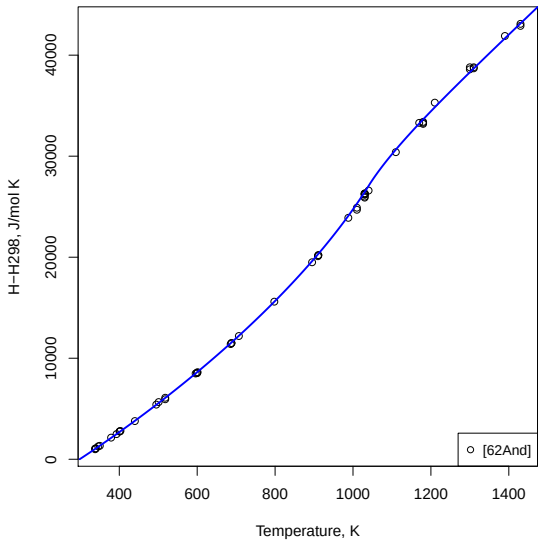

Figure 22: Calculated and experimental relative enthalpy $H - H_{298.15}$ for pure Fe

Reference	method	details	Cr bcc	Fe bcc	Al fcc
Dinsdale (1991) [8]		assessed	23.54	27.28	28.30
Palumbo (2013) [20]	QE	calc.QHA	23.07	26.58	27.42
		calc.QHA+el.	23.72	27.41	27.70
	VASP	calc.QHA	23.03		
		calc.QHA+el.	23.50		
Present work	NLS	SR with Debye	24.02	28.18	28.46
		SR with Einstein	23.34	27.51	27.69
		CS with Debye	24.03	28.24	28.47
		CS with Einstein	23.24	27.54	27.73
		RW with Debye	24.41	28.23	28.44
		RW with Einstein	23.60	27.51	27.66

Table 9: Calculated standard entropy $S_{298.15}$

for the relative entropy are obtained by application of the models (6), (7) and (8) with the Debye function for description of the phonon contributions. Comparison between experimental and calculated relative enthalpy $H(T) - H_{298.15}$ is shown in Fig. 20 and delivers good agreement from the room temperature, 298.15K, up to the high temperatures. No data on the relative enthalpy at the temperatures below $298.15K$ were found in the literature.

4 Conclusion

A novel physically-based segmented model for the description of the thermodynamic properties of the pure elements down to 0K has been proposed, which is based on a combination of a statistical fit of the heat capacity data with several physical models. The thermodynamic properties of pure Cr, Al and Fe have been modeled by a segmented regression model and the proposed method provides very good prediction of experimental data. The new segmented model has been compared with already existing physically-based formulations and it is demonstrated for all selected pure elements that it is most appropriate for the description of the heat capacity data with respect to to several statistical criteria, which measure the quality of a statistical fit to experimental data.

Acknowledgements

Collection of experimental data from available literature is very tedious and time consuming process and authors would like to thank Dr. Mauro Palumbo and Dr. Suzana G. Fries from Computational Thermodynamics/CALPHAD research group, Interdisciplinary Center for Advance Material Simulation (ICAMS), for providing the experimental data of the selected elements.

This work has been supported in part by the Collaborative Research Center "Statistical modeling of nonlinear dynamic processes" (SFB 823, Project C1) of the German Research

Foundation (DFG) and by the Collaborative Research Center "Superalloys Single Crystal" (TR-103 project C6). Also we would like to acknowledge the financial support from Sino-German Cooperation Group GZ 755 "Microstructure in Al Alloys".

References

[1] C. Travis Anderson. The heat capacities of chromium, chromic oxide, chromous chloride and chromic chloride at low temperatures. *Journal of the American Chemical Society*, 59(3):488–491, 1937.

[2] J.-O. Andersson. Thermodynamic properties of chromium. *International journal of thermophysics*, 6(4):411–419, 1985.

[3] Florent Baty and Marie-Laure Delignette-Muller. *nlstools: tools for nonlinear regression diagnostics*, 2013. R package version 0.0-15.

[4] Sedigheh Bigdeli, Huahai Mao, and Malin Selleby. On the third-generation calphad databases: An updated description of Mn. *Physica Status Solidi (b)*, 252(10):2199–2208, 2015.

[5] Malcolm W. Chase, Ibrahim Ansara, Alan Dinsdale, Gunnar Eriksson, Goran Grimvall, Lars Hoglund, and Harumi Yokokawa. Group 1: Heat capacity models for crystalline phases from 0 K to 6000 K. *Calphad: Computer Coupling of Phase Diagrams and Thermochemistry*, 19(4):437–447, 1995.

[6] Qing Chen and Bo Sundman. Modeling of thermodynamic properties for Bcc, Fcc, liquid, and amorphous iron. *Journal of Phase Equilibria*, 22(6):631–644, 2001.

[7] K. Clusius and P. Franzosini. Ergebnisse der tieftemperaturforsdiung xxxviii: Atom- und elektronenwrme des chroms zwischen 14k und 273k. *Z. Naturforschg.*, 17a:522–525, 1962.

[8] A.T. Dinsdale. Sgte data for pure elements. *Calphad*, 15(4):317–425, October 1991.

[9] A. E. Dubinov and A. A. Dubinova. Exact integral-free expressions for the integral Debye functions. *Technical Physics Letters*, 34(12):999–1001, 2008.

[10] I. Estermann, S.A. Friedberg, and J.E. Goldman. The specific heats of several metals between 1.8 and 4.2 k. *Physical Review*, 87(4):582, 1952.

[11] Brandon M. Greenwell. *investr: Inverse Estimation / Calibration Functions*, 2015. R package version 1.3.0.

[12] G. Grimvall. *Thermophysical properties of materials.* Amsterdam: North Holland, 1986.

[13] G. Grothendieck. *nls2: Non-linear regression with brute force*, 2013. R package version 0.2.

[14] I. I. Guseinov and B. A. Mamedov. Calculation of integer and noninteger n-dimension debye functions using binomial coefficients and incomplete gamma functions. *International Journal of Thermophysics*, 28(4):1420–1426, 2007.

[15] Mats Hillert and Magnus Jarl. A model for alloying in ferromagnetic metals. *Calphad*, 2(3):227–238, 1978.

[16] F. Koermann, B. Grabowski, P. Soederlind, M. Palumbo, S. G. Fries, T. Hickel, and J. Neugebauer. Thermodynamic modelling of chromium: strong and weak magnetic coupling. *Journal of Physics: Condensed Matter*, 25, 2013.

[17] D. Levant, R. Moreh, and O. Shahal. Testing the phonon spectrum of metallic chromium with the nuclear-resonance photon scattering technique. *Physical Review B*, 44(1):386, 1991.

[18] Hans Leo Lukas, Suzana G. Fries, and Bo Sundman. *Computational thermodynamics: the Calphad method*, volume 131. Cambridge university press, 2007.

[19] Reza Naraghi, Malin Selleby, and John Agren. Thermodynamics of stable and metastable structures in Fe–C system. *Calphad*, 46:148–158, 2014.

[20] M. Palumbo, B. Burton, A. CostaeSilva, B. Fultz, B. Grabowski, G. Grimvall, B. Hallstedt, O. Hellman, B. Lindahl, A. Schneider, P. E. A. Turchi, and W. Xiong. Thermodynamic modelling of crystalline unary phases. *Physica Status Solidi (b)*, 251(1):14–32, 2014.

[21] R Core Team. *R: A Language and Environment for Statistical Computing*. R Foundation for Statistical Computing, Vienna, Austria, 2013. ISBN 3-900051-07-0.

[22] J.A. Rayne and W.R.G. Kemp. Xciii. the heat capacities of chromium and nickel. *Philosophical Magazine*, 1(10):918–925, 1956.

[23] C. Ritz and J. C. Streibig. *Nonlinear regression with R*. Springer, 2008.

[24] G. A. F. Seber and C. J. Wild. *Nonlinear regression*. Wiley, New York, 1989.

[25] N.M. Wolcott. The specific heat of transition metals. *Conf.de Physique des Basses Temperatures, Paris*, page 286, 1955.

[26] Wei Xiong, Qing Chen, Pavel A. Korzhavyi, and Malin Selleby. An improved magnetic model for thermodynamic modeling. *Calphad*, 39:11–20, December 2012.

[27] Wei Xiong, Peter Hedstrm, Malin Selleby, Joakim Odqvist, Mattias Thuvander, and Qing Chen. An improved thermodynamic modeling of the Fe-Cr system down to zero kelvin coupled with key experiments. *Calphad*, 35(3):355–366, 2011.